Available online at www.sciencedirect.com
SCIENCE DIRECT®
Journal of Photochemistry and Photobiology A: Chemistry 163 (2004) 331–340
Journal of Photochemistry and Photobiology A:Chemistry
www.elsevier.com/locate/jphotochem

Comparative studies of substituted ruthenium(II)–pyrazoyl–pyridine complexes with classical N3 photosensitizer: the influence of –NCS dye ligands on the efficiency of solid-state nanocrystalline solar cells

T. Stergiopoulos [a,b], S. Karakostas [b], P. Falaras [a,*]

[a] *Institute of Physical Chemistry, NCSR "Demokritos", 153 10 Aghia Paraskevi, Attikis, Athens, Greece*
[b] *SOLAR TECHNOLOGIES S.A., Viomichaniki Periochi Ioanninon, 45500 Ioannina, Greece*

Received 20 November 2003; received in revised form 20 November 2003; accepted 7 January 2004

Abstract

New dyes of the type [Ru(II)(bdmpp)(dcbpy)X](PF_6) (where bdmpp is 2,6-bis(3,5-dimethyl-*N*-pyrazoyl)pyridine, dcbpy is 2,2′-bipyridine-4,4′-dicarboxylic acid and X = Cl^- (Ru–Cl) or NCS^- (Ru–NCS)) have been tested with success as molecular antennas in titania nanocrystalline photoelectrochemical cells (DSSCs) and compared with the Grätzel's N3 photosensitizer, in modules fabricated using a composite polymer solid-state electrolyte The solar cells made using the complex with the –NCS ligand have a significantly better performance than those fabricated with the dye containing the Cl^- ligand. The comparison of their action spectra has revealed that the Ru–NCS dye presents higher incident monochromatic photon-to-current conversion efficiency (IPCE) values. The Ru–NCS cells produced a short-circuit photocurrent as high as 4.3 mA cm^{-2} and an open-circuit photovoltage of 584 mV, which led to an overall energy conversion cell efficiency (η) as high as 1.64%, about three times higher than the corresponding efficiency obtained with Ru–Cl dye. On the basis of the obtained results the energetic diagrams of the corresponding DSSCs were constructed. The observed differences are attributed to the contribution of the isothiocyanato group on the light absorption, on the redox properties and on the increase of the charge injection efficiency. A gain in photovoltaic performance of the –NCS containing dyes is also proposed through a reduction of the dark current of the corresponding solid-state solar cells.

Keywords: Ru(II)-bdmpp-dcbpy complexes; TiO_2 films; NCS ligands; Composite PEO-titania-I^-/I_3^- electrolyte; Solid nanocrystalline solar cell

1. Introduction

The most efficient charge transfer sensitizers employed so far for dye sensitized nanocrystalline TiO_2 solar cells (DSSCs) are polypyridyl-type complexes of ruthenium(II) [1]. Ten years ago, the dye *cis*-$Ru(NCS)_2(dcbpy)_2$ (N3) has been synthesized and incorporated in a photoelectrochemical cell which reached a 10% (under AM 1.5 illumination) solar-to-electric conversion yield [2]. Thereafter, only the Grätzel group has synthesized more than 800 dyes, but no one was able to reach the outstanding performance of the N3 dye [3]. Only recently, a black dye tris(isothiocyanato)-2,2′,2″-terpyridyl-4,4′,4″-tricarboxylate) ruthenium(II) was proved to exhibit similar photovoltaic properties with the N3 dye [4].

These results raised the question as to why these two dyes are the more efficient molecular antennas in nanocrystalline photoelectrochemical cells. In both cases, the fundamental idea was to use a chromophoric ligand with low-lying π^*-orbitals (dcbpy or terpy) that possess –COOH anchoring groups to firmly adsorb on the semiconductor surface, together with another ligand (–NCS) that controls the redox properties of the ground (HOMO) and excited (LUMO) states of the dyes. Consequently, the two photosensitizers showed intense metal to ligand charge tranfer transitions (MLCT) extended into very low energies (almost near IR photoresponse). These transitions led to the creation of long-lived excited states that had the driving force to quickly inject all their electrons into the TiO_2 conduction band (a practical 100% quantum efficiency). Moreover, all the parallel reactions that take place in a regenerative cell, involving the sensitizer, were certainly favored. That is, the rate of reduction of the oxidized form of the dye from the redox couple was increased, while the probability of

* Corresponding author. Tel.: +30-210-6503644; fax: +30-210-6511766.
E-mail address: papi@chem.demokritos.gr (P. Falaras).

1010-6030/$ – see front matter © 2004 Elsevier B.V. All rights reserved.
doi:10.1016/j.jphotochem.2004.01.002

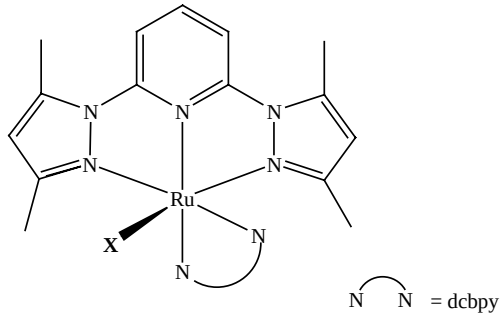

Fig. 1. Molecular structure for the Ru–Cl and Ru–NCS complexes.

the excited electron to recombine before reaching the back contact was diminished.

Trying to design molecular sensitizers for photoelectrochemical applications, our laboratory has synthesized a new ruthenium complex [Ru(II)(bdmpp)(dcbpy)Cl](PF_6), abbreviated Ru–Cl, and then –Cl has been replaced by the less electronegative ligand, –N=C=S). That is, the complex turned out to be [Ru(II)(bdmpp)(dcbpy)(NCS)](PF_6), abbreviated Ru–NCS (the molecular structures of the dyes are shown in Fig. 1). Both complexes contain a typical pyridine group (dcbpy = 2,2′-bipyridine-4,4′-dicarboxylic acid) that bears a carboxylic acid functional moiety, which serves as interlocking agent. The above dyes also possess a pyrazole ligand [bdmpp = 2,6-bis(3,5-dimethyl-*N*-pyrazoyl)pyridine], which can be considered as a terpyridine derivative, exhibiting though significantly different electronic properties. The terdentate binding nature and resulting strong chelate effect of the latter ligand inhibits ligand loss that can take place for analogous monodentate complexes. Additionally, bdmpp typically occupies three meridional coordination sites producing octahedral complexes that are not stereochemically active [5]. The combination and co-existence of mixed azo-aromatic ligands with well optimized π^* energies, together with an appropriate ancillary ligand is expected to extend the dyes light harvesting ability and tune their redox properties [6].

In this paper, we present our results on the spectrophotoelectrochemical properties of nanocrystalline TiO_2 thin films, successfully sensitized by the above mentioned dye molecules. These photoanodes were incorporated in solid-state solar cells, using a composite electrolyte consisting of high-molecular mass polyethylene oxide (PEO) with the addition of a "solid plasticizer" (commercial TiO_2) in the presence of the I^-/I_3^- redox couple [7]. Such a composite material is particularly attractive because it permits excellent ionic mobility of the iodide/tri-iodide anions in its solid-state matrix [8]. The photoelectrochemical properties of the new complexes are compared with those taken by standard N3 dye in terms of the different chemical properties of the ligands attached to the central metal. The obtained results confirm that –NCS ligand has a positive influence on the light absorption and charge transfer properties of the complex and hence in the photovoltaic performance of the corresponding solar cells [9].

2. Experimental

2.1. Titania thin film electrodes

Opaque, nanostructured TiO_2 films were prepared using the doctor-blade technique on TEC15 conductive glass substrates (purchased from Hartford Glass Co. Inc.). A viscous paste was first prepared according the method described in ref. [10] and the resulting dispersion was smeared by a glass rod onto the TEC15 substrate. An adhesive tape strip on the conductive glass determines the film thickness. The layer was thermally treated at 450 °C at a rate of 20 °C min^{-1} for 30 min in order to ensure good adhesion to the substrate and electrical contact (sintering) between the nanoparticles. The film thickness was typically 5 μm and uniform all over the films' extension as evaluated by surface profilometry.

2.2. Chemical attachment of the dyes on the oxide surface

The two bdmpp dyes were synthesized according the previously described procedures [11,12]. N3 dye (or Ru535) was purchased from Solaronix. Dyes grafting on the titanium oxide was achieved by immersing the thin film electrodes overnight in a 10^{-4} M alcohol solution of the complexes. Noteworthy that a deep yellow brown color for the bdmpp complexes (whilst a dark red color was appeared for N3 dye) was developed imminently after immersion, confirming the dyes attachment on the semiconductor surface. Any dye in excess was eliminated by thoroughly washing and thus, a monolayer coverage of the oxide surface was assured [13].

2.3. PEO/TiO_2/I^-/I_3^- composite electrolyte

For the polymer electrolyte preparation, TiO_2 Degussa P25 powder (about 9%, w/w) was first dispersed in CH_3CN. To this dispersion, the I^-/I_3^- redox couple was incorporated. Then, polyethylene oxide (63%, w/w) was added under continuous stirring. The final product was heated in order to evaporate the solvent. DSC thermograms confirmed the high amorphicity of the composite polymer electrolyte [7].

2.4. Device assembly

Solid-state solar cells of lamellar structure were fabricated by sandwiching the composite polymer electrolyte between the derivatized titania photoelectrode (TEC15/TiO_2/dye) and

a (TEC15) counter electrode coated with a thin layer of platinum to catalyze the iodide regeneration.

2.5. Characterization techniques

UV-Vis reflectance spectra of the modified films were obtained with a Hitachi U-4001 spectrophotometer equipped with an integrating sphere in order to avoid light scattering effects. The experimental technique for measurements of the incident monochromatic photon-to-current conversion efficiency (IPCE), which is commonly used for measurements on DSSC [14], consists of illuminating the cell with constant bias light in combination with a monochromator, where 10% of the exciting light intensity is modulated and the resulting modulated photocurrent is detected by a frequency response analyzer. Further details for the experimental set-up, one can find in ref. [15].

Current–voltage (*I–V*) characteristics were obtained under full sunlight illumination by connecting the cell to a variable resistor together with a microampere meter in series and a voltmeter in parallel. The sunlight illumination intensity was directly measured using a 28-0925 ealing research radiometer–photometer operating in conjunction with a 28-0982 silicon detector and a 28-0727 flat response filter. Dark *I–V* measurements were realized by performing a cyclic voltamogram at a sweep rate of $20\,mV\,s^{-1}$, using an Autolab potentiostat (Eco Chemie) operating in two-electrodes mode, controlled by a personal computer.

For all experiments, a batch of 10 cells was tested and a mean value for the obtained results has been taken into account. Repeated measurements yielded reproducible values, so that this statistical treatment provided a very representative outcome for our analysis.

3. Results and discussion

3.1. Electronic spectra of sensitized TiO_2 electrodes

The electronic spectra of the complexes Ru–Cl and Ru–NCS in solution (left Fig. 2a and b, respectively), present a quasi-similar behavior with three absorption maxima of very high intensity ($>20000\,M^{-1}\,cm^{-1}$) in the visible attributed to metal-to-ligand charge transfer processes. It is also worth to mention the presence of an absorption hump at about 570 nm for both dyes. These MLCT transitions involve separate excitations from a d-orbital of the metal to a π^*-orbital of a ligand. Then, the excitation energy is rapidly channeled into the ligand having the lowest π^*-acceptor orbitals and is the one from which electron injection into the conduction band takes place [16]. The spectrum of Ru–NCS is obviously blue-shifted compared with N3 spectrum although it presents significantly higher absorbance extinction coefficients. The above dissimilarities verify that the bdmpp ligand is involved in the MLCT transitions and that this ligand is a weaker acceptor than dcbpy. Halide ions like –Cl are stronger σ- and π-donors than the –NCS ligands and someone would expect a blue shift in the absorbance spectra of Ru–NCS dye in comparison with Ru–Cl complex. However, one notices a slight red-shift (about 10 nm) due to the extent of π-back donation to the isothiocyanato ligand from Ru(II) center [2].

The absorbance spectra of the dye-sensitized TiO_2 films (after subtraction of background absorption from the TiO_2/TEC15 alone) reveal that the modified electrodes exhibit strong and broad absorption in the visible, centered at 463 nm (right Fig. 2a and b, for Ru–Cl/TiO_2 and Ru–NCS/TiO_2, correspondingly). Besides their high intensity, the spectra for the two photoelectrodes are almost

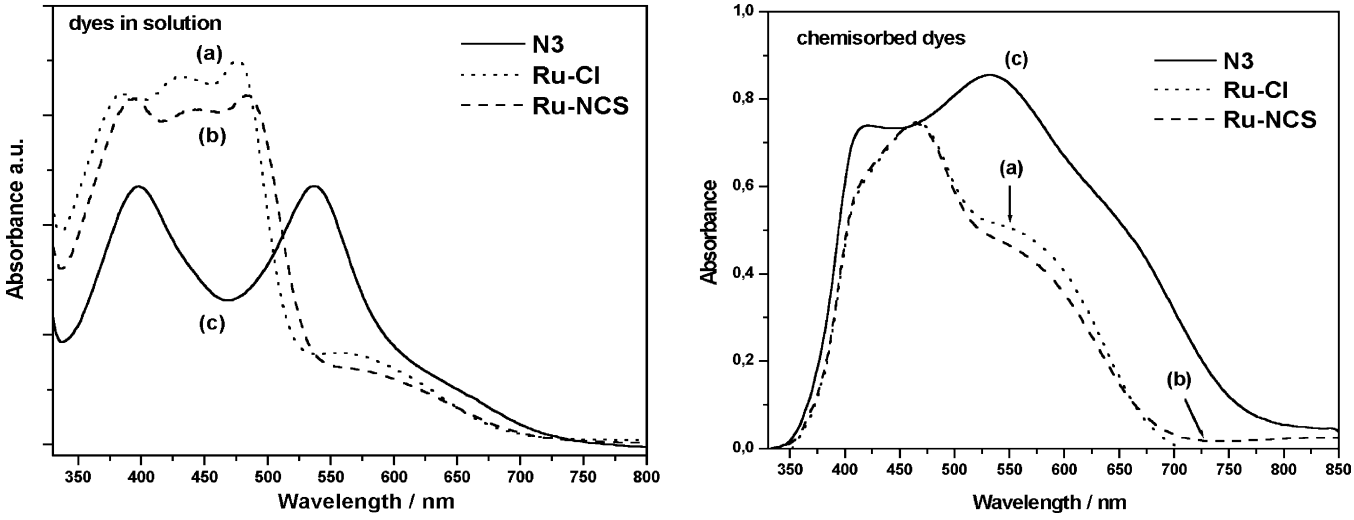

Fig. 2. Left: absorbance spectra in alcohol solution for the dyes Ru–Cl (a), Ru–NCS (b), and N3 (c), respectively. Right: absorption spectra of TiO_2 obtained after modification with the dyes Ru–Cl (a) and Ru–NCS (b), and the corresponding spectrum of TiO_2 treated with N3 dye (c) is presented for comparison.

identical and cover a good part in the visible region, but the spectrum of the second film sensitized by the second dye also expands with a somewhat longer tail up to around 730 nm. The slight change in the tail of the absorption spectra shows that the low energy MLCT transition is very little influenced by the presence of a π^* low-lying orbitals ligand like –NCS. This change is not observed in the solution probably because of the dependence of the spectra on the solvent (a probable exchange of the anionic ligand with a neutral solvent molecule may slighly shift a MLCT band). The fact that the absorbance spectra of the modified titania thin film photoelectrodes are broader than the electronic spectra of the dyes in methanol can be explained by a large change in the energy levels of HOMO and LUMO of the complexes. This is probably due to the strong interaction between the dye molecules and the TiO_2 substrate and confirms the chemical binding of the sensitizers to the semiconductor surface via the formation of an ester-like linkage between the dye molecules and the hydroxylated titania surface [17].

3.2. Incident photon-to-current efficiency

Photocurrent action spectra obtained with the titania films coated with monolayers of the Ru–Cl and Ru–NCS complexes are shown in Fig. 3a and b, respectively, where the incident photon-to-current conversion efficiency is plotted as a function of the incident wavelength. The data were obtained under short-circuit conditions measured at $\sim 10^{14}$ photons $cm^{-2}\,s^{-1}$ (intensity of dc illumination). IPCE represents the percentage of incident photons that are converted to electrons reaching the TEC15 conducting substrate at a certain wavelength and is defined by the formula:

$$\mathrm{IPCE}(\lambda) = 1239 \times \left(\frac{I_\lambda(\mu A\,\mathrm{cm}^{-2})}{\lambda(\mathrm{nm}) \times P_\lambda(W\,\mathrm{m}^{-2})} \right) \quad (1)$$

where I_λ is the short-circuit photocurrent intensity, λ the wavelength, and P_λ is the incident radiative flux [18].

Typical maximum IPCE values at the absorption maximums of Ru–Cl dye in solution are easily distinguished in the action spectrum, around 30% at 400 and 440 nm, whilst at 470 nm the IPCE value is 28%. The photocurrent generation threshold is at about 570 nm. On the contrary, the use of the Ru–NCS dye clearly reveals a plateau, about 36%, in the wavelength region between 400 and 480 nm (an IPCE max of 38% was reached at 470 nm), while the IPCE is almost constant (about 22%) in the wavelength area from 480 to about 600 nm. The obtained values for the latter dye were about 60% of the values attained with N3 dye in the same region, left Fig. 3c. Yet, the IPCE value for N3 dye at 470 nm was 62% and it was increased up to 65% after 480 nm. Moreover, a 35% photocurrent generation efficiency was retained even at 600 nm. The clear superiority of the N3 dye (neutral molecule) with respect to the two new dyes can result from a minimal dye loading attributed to the positive charging of these complexes (Ru–NCS and Ru–Cl), which may influence their interaction with the semiconductor surface in a harmful way, since the adsorbed species are expected to show lateral Coulombic repulsion [4].

Still, the IPCE values found for all complexes seem rather low when compared with others found in literature (for example, see ref. [19]). In the light of the above postulation, one can argue that the efficiency of collecting the injected charge (p_c) at the back contact is not 100%, especially when using low intensity illumination. Fisher et al. [20] have found a slight variation of IPCE of about 35%, when diverge the incident photon current density over 5 orders of magnitude down to very low values in the range of 10^{10} photons $cm^{-2}\,s^{-1}$. On the other hand, Trupke et al. [14] have observed that p_c decreases strongly at low absorbed photon current densities $<10^{16}$ photons $cm^{-2}\,s^{-1}$ due to the loss

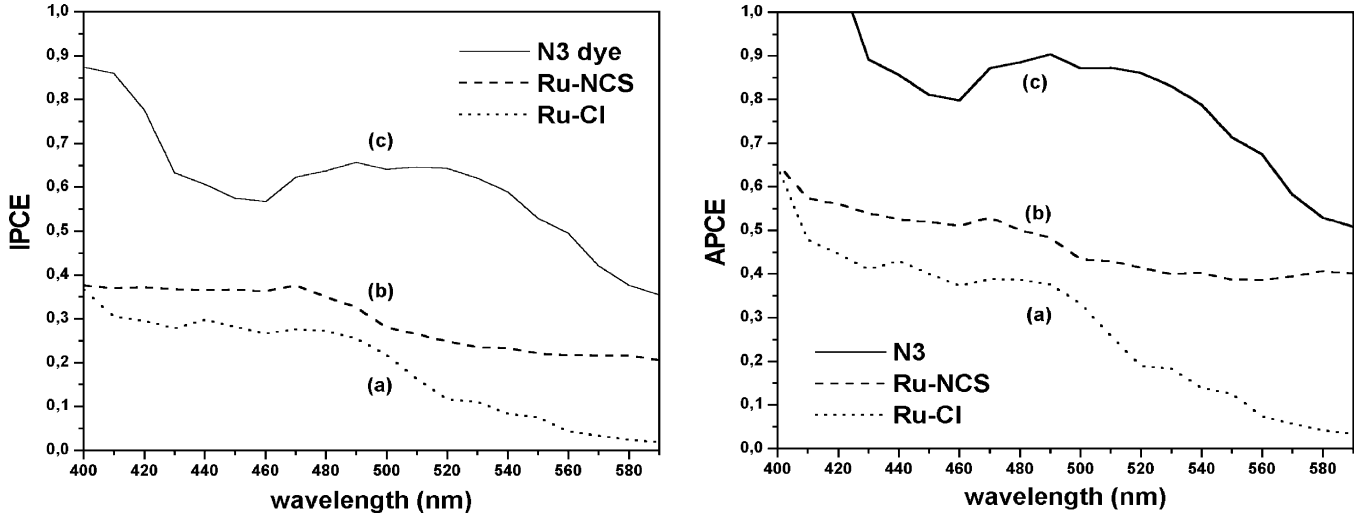

Fig. 3. Left: photocurrent action (IPCE) spectra of the TiO_2/Ru–Cl dye (a), TiO_2/Ru–NCS dye (b) DSSCs with illumination through the conductive substrate together with the corresponding IPCE spectrum of N3 dye (c) for comparison. Right: APCE spectra of the TiO_2/Ru–Cl dye (a), TiO_2/Ru–NCS dye (b), and TiO_2/N3 dye (c) films.

of photogenerated electrons via surface-state-mediated electron transfer into the electrolyte. Our group has studied the influence of the incident photon flux between $\sim 10^{14}$ and 10^{16} photons $cm^{-2}\,s^{-1}$ on IPCE values [21] and also found a variation of about 30%. Hence, one might state that measuring the IPCE values of the complexes at 10^{14} photons $cm^{-2}\,s^{-1}$ results in an underestimation of the IPCE.

3.3. Electron transfer yield (APCE)

In order to rationalize all the findings observed from IPCE measurements, the monochromatic current yield (IPCE) is expressed in terms of light harvesting efficiency (LHE) (λ), the quantum yield of charge injection (ϕ_{inj}), that is, the probability that the excitation of an adsorbed dye molecule leads to electron injection into the TiO_2 conduction band, and the collection efficiency (p_c), which is the probability that the injected electron contributes to the current through the external circuit:

$$\mathrm{IPCE} = \mathrm{LHE}(\lambda)\varphi_{inj}\,p_c \tag{2}$$

The product of the electron injection yield and the charge collection efficiency can be further expressed as an electron transfer yield, $\Phi_{ET}(\lambda)$ [2]:

$$\phi_{ET}(\lambda) = \varphi_{inj}\,p_c \tag{3}$$

The electron transfer yield is also frequently expressed as an absorbed photon-to-current conversion efficiency (APCE) and thus can be calculated from the following equation [22]:

$$\mathrm{APCE}(\lambda) = \frac{\mathrm{IPCE}(\lambda)}{\mathrm{LHE}(\lambda)} \tag{4}$$

Taking into account the absorbance for the chemisorbed dye molecules Abs (λ) (right Fig. 2), one can obtain the fraction of the incident light absorbed by each dye on every wavelength, LHE (λ) [2]:

$$\mathrm{LHE}(\lambda) = 1 - 10^{-\mathrm{Abs}(\lambda)} \tag{5}$$

Using Eq. (4), the absorbed photon-to-current conversion efficiency APCE can be easily calculated for every wavelength and the spectra were plotted in right Fig. 3. Note that the initial IPCE values were corrected for 15% reflection and absorption losses of the conducting glass (3 mm thick), serving as a support for the opaque TiO_2 film. In Fig. 3, one can see that, in the case of the new dyes, a large percentage of the absorbed photons are not converted to conducting electrons in the external circuit. The Ru–Cl dye loses about the 60% of the absorbed photons in the region where its light harvesting efficiency is high (400–500 nm). On the other hand, the second Ru–NCS dye has around 45% losses at the same region, while it presents a quasi plateau in the region 500–600 nm. As for N3 dye, one can easily observe its large ability (almost unity) in an extent wavelength area to transfer all the excited electrons at the rear contact. The observed differences in injection quantum yields (APCE) can be ascribed either to differences in electron injection efficiencies or in charge recombination dynamics (see Eq. (3)). Even if dissimilarities in charge recombination kinetics will be revealed in the following sections, we must admit that recombination cannot affect to a great extent the APCE values at short-circuit. Then, one can assign the observed ABCE behaviour to differences in charge injection efficiency the latter being the only parameter that is wavelength dependent [23]. Especially in the spectral domain where the light harvesting efficiencies are equal, the observed superiority of Ru–NCS against Ru–Cl dye results from differences more likely in electron injection efficiencies (ϕ_{inj}) rather than in charge collection efficiency (p_c). One can assume that the –NCS ligand coordinated into ruthenium forms longer-lived excited states than –Cl ligand does, improving charge injection. Nevertheless, the new complexes contain bdmpp ligands that already have relatively short-lived MLCT states as the analogous terpy complexes [24]. Furthermore, direct electron injection to the conduction band from a remote ligand [25], which contains π^* low-lying orbitals (like –NCS) might take place. Aggregation of the sensitizer molecules can affect the injection quantum yield [26], but since the absorption spectra on TiO_2 of all dyes is different than that of the dyes in solution (e.g. aggregation takes place on the surface), we cannot quantify, for all three types of DSSC, the percentage of inactive dyes that are unable to inject electrons in the conduction and relate it with the observed differences in APCE values. The coordination of a π^* low-lying orbitals ligand like –NCS to a metal complex can affect the processes of intramolecular reorganization of excitation energy in different Franck–Condon states (by defining the energetics of singlet or triplet excited states [23]) in a way that additional states would effectively inject electrons in TiO_2.

3.4. I–V characteristics of regenerative cells

Fig. 4 exhibits the current–voltage characteristics of the dye-sensitized solar cells employing the composite polymer electrolyte, measured under direct solar illumination (solar irradiance was $656\,W\,m^{-2}$). By using the Ru–Cl dye, the solid-state photoelectrochemical cell produced a continuous short-circuit photocurrent (I_{sc}) as high as $1.38\,mA\,cm^{-2}$, and an open-circuit photovoltage (V_{oc}) of 491 mV, Fig. 4a. The fill factor (FF) defined as:

$$\mathrm{FF} = \frac{V_{opt}I_{opt}}{V_{oc}I_{sc}} \tag{6}$$

where V_{opt} and I_{opt} are, respectively, voltage and current for maximum power output, was calculated to be 0.46. The overall energy conversion efficiency (η) is defined as follows:

$$\eta = \frac{I_{sc}V_{oc}\mathrm{FF}}{P_{in}} \tag{7}$$

where P_{in} stands for the power of the incident illumination. The cell showed clearly low performance with an overall energy conversion efficiency of 0.48%.

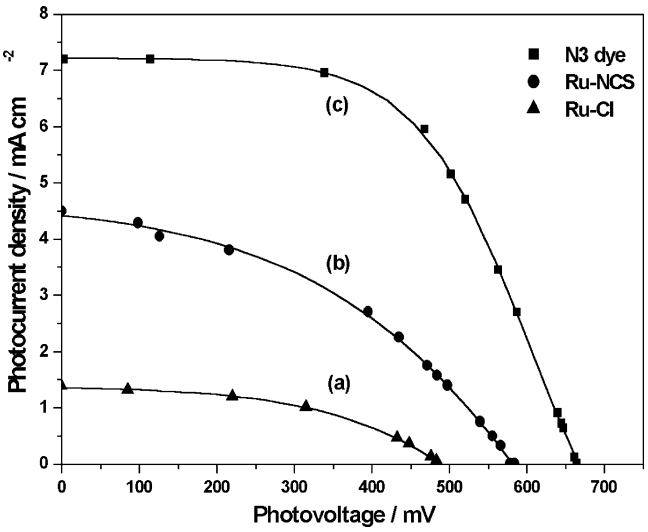

Fig. 4. Current–voltage characteristics under illumination of the TiO_2/Ru–Cl (a), Ru–NCS (b), and nanocrystalline solar cells using the PEO/TiO_2 composite electrolyte, comparing with the standard complex N3 (c). Area: 0.42 cm^2, solar irradiance: 65.6 mW cm^{-2}.

However, significantly better performance was observed using the Ru–NCS dye, Fig. 4b. The corresponding values obtained under similar conditions were: a short-circuit current density $J_{sc} = 4.29\,mA\,cm^{-2}$, an open-circuit photovoltage $V_{oc} = 584\,mV$, a fill factor FF = 0.43, and finally an energy conversion efficiency η of 1.64%. As one can see, the considerable increase of the overall efficiency is due to the ∼90 mV difference in open-circuit photovoltage between the two dyes but mainly it is credited at the about three times rise of the short-circuit photocurrent. Still, the above energy conversion efficiency is about the 40% of the efficiency obtained with the standard N3 dye ($\eta = 4.2\%$), corresponding to the 60% of the short-circuit photocurrent ($I_{sc} = 7.2\,mA\,cm^{-2}$), the 88% of the open-circuit photovoltage ($V_{oc} = 664\,mV$) and finally 74% of the corresponding fill factor (FF = 0.58) obtained with N3 [8]. The relatively poor values of fill factor, decreasing to a large extent the overall energy conversion efficiency, are probably due to an insufficient wetting of the photoelectrode pores by the solid electrolyte.

From the above results, one can end that the superiority of the N3 dye with respect to the two new dyes mainly results from a large increase of the short-circuit photocurrent, accounted for higher external quantum yields (IPCE). Note that the short-circuit photocurrent is the overlap of the IPCE action spectrum with the solar spectrum. The higher values of IPCE are attributed to higher light harvesting efficiencies and electron injection efficiencies (ϕ_{inj}), especially in the (500–600 nm) wavelength region. This also explains the differences between the two new dyes. One can admit that the increase of the short-circuit photocurrent for the Ru–NCS dye comparing with the Ru–Cl dye corresponds to the higher APCE values of the former dye, especially in the 500–600 nm region where the latter dye's efficiency is very low (right Fig. 3).

The difference in V_{oc} (the photovoltage measured under open-circuit conditions) for the three dyes can be considered as a strange result, if one takes into account the exact concept of the photovoltage in dye-sensitized solar cells. That is, the maximum photovoltage that one can obtain in a DSSC doesn't involve the dye ground and excited states and is the change in the electrochemical potential of electrons in the TiO_2 from its value in the dark [27]. Hence, someone could state that all the dyes should provide an identical photovoltage. However, one must take into consideration the following equation, holding for V_{oc} [28]:

$$V_{oc} = \left(\frac{mRT}{F}\right) \ln\left(\frac{I_{sc}}{i_0} - 1\right) \tag{8}$$

where m is the ideality factor whose value is between 1 and 2 for DSSC [29], I_{sc} the short-circuit photocurrent, i_0 the reverse saturation current (or dark current), and R and F are the ideal gas and Faraday's constant, respectively.

The obtained values of V_{oc} for all three dyes are much smaller than the maximum theoretical predicted values. Taking into consideration the E_{ox} of the I^-/I_3^- couple ∼+0.2 V versus SCE [30] and the reported values of E_{cb} for TiO_2 (−0.7 V versus SCE) [31], the cells should furnish maximum photovoltage of about 900 mV. Even if the actual band edge position may be somewhat different when in contact with the solid redox electrolyte, the voltage decrease can be only explained by taking into account charge recombination. From Eq. (8), one can deduce the main parameters influencing the magnitude of V_{oc} values. These aspects will be thoroughly discussed in the following section.

3.5. Effect of the applied voltage-dark current

Current–voltage curves in the dark, Fig. 5, were obtained by performing linear sweep cyclic voltammetry (CV) (the scan rate $s = dV/dt$ remains constant) using a two electrodes arrangement in an electrochemical window from −0.0 to −0.6 V. A rapid rise of the cathodic current can be identified at about −250 mV for all three complexes. The two curves, involving Ru–Cl and Ru–NCS dyes (Fig. 5a and b), have the same shape, whereas the –Cl replacement by –NCS in the complex induces a shift of the curve to negative potentials. The obvious reduction of dark current enhances the open-circuit photovoltage of the second cell by about 90 mV. In a regenerative solar cell, the dark current flowing in the external circuit is usually originated from the reduction of species present in the electrolyte [32]. Hence, the obtained dark curves are mainly attributed to the following equilibrium reaction, i.e. charge recombination at the nanocrystalline/redox electrolyte interface [33]:

$$I_3^- + 2e^- \rightarrow 3I^- \tag{9}$$

In fact, the above reduction of triiodide by conduction band electrons at the surface of the dye-sensitized TiO_2 photo-

electrodes was found to make the major contribution to the dark current during the cell operation [34] (electron injection from the partly exposed SnO_2:F substrate to the triiodide through the porous TiO_2 layer is established to be a trivial phenomenon [35]).

Such a presence of large values of dark current leads to photovoltage losses (see Eq. (8)), and thus, minimization of the overall efficiency of DSSCs. The reverse current's reduction may result from a displacement of the equilibrium Eq. (9) to the left. Greijer Angrell et al. [36] have proposed that a complex between iodine or triiodide and –NCS ligand is formed during the cell operation and consequently this side reaction would displace Eq. (9) towards producing I_3^- anions, and thus, it would minimize the opposite reaction (dark current generation). In the case of N3 dye, which in turn contains two –NCS ligands, the curve is shifted again at negative potentials by about 80 mV (Fig. 5c), confirming the above assumption.

3.6. Recombination effects

In Fig. 4, one can see that, despite N3, there is no net photocurrent plateau for Ru–Cl and Ru–NCS dyes close to short-circuit (0, ∼−0.18 V). Even if subtracting the curves in the dark (Fig. 5) from these under illumination (Fig. 4), we can state that there are still recombination centers decreasing the predicted photocurrent plateau in the above region. Note that the dark current is almost zero at this region. Despite the effect of the high internal series (the magnitude of ohmic drops are of the order of 100 Ω cm^{-2} for all solid-state solar cells, obtained from impedance measurements) and the difference in fill factor values (about 23% larger in the case of N3), the observed unusual behavior could be attributed to the recombination reactions taking place when the injected electron is trying to reach the rear contact:

$$Ru^{2+*} \rightarrow Ru^{2+} \quad (10)$$

$$Ru^{3+} + TiO_2(e^-) \rightarrow Ru^{2+} + TiO_2 \quad (11)$$

Eq. (10) expresses the probability of the dye to decay to the ground state after excitation and is directly correlated with the opposite of charge injection efficiency (ϕ_{inj}). On the other hand, Eq. (11) illustrates the direct recombination of the injected electron to the TiO_2 conduction band with the hole left in the HOMO of the dye [37]. Unfortunately, we are not experimentally able to identify which way of recombination is the predominant. Concerning the first reaction, Tachibana et al. [38] have concluded that the bias dependence of the injection kinetics (even close V_{oc}) is unlikely to play a key role in limiting the photocurrent generated from a DSSC. Note that the discussed region close to short-circuit is related to very small negative applied potentials far away from V_{oc}. Thus, we can assume that the recombination of the conduction band electrons with the oxidized dye, Eq. (11) plays a significant role on the dynamics of the TiO_2 solar cells sensitized by Ru–Cl and Ru–NCS dyes. On the contrary, in the case of N3 dye solar cell (apparent photocurrent plateau, Fig. 4c), the above reaction does not seem to be significant, at least near the photocurrent plateau region. This proves that the superiority of N3 dye is in part explained by the tuning of the charge recombination kinetics of DSSCs. As already stated by Rensmo et al. [39], the positive charge density of the cation state of N3 dye is located on the ruthenium and NCS moieties of the complex (comprising the HOMO levels of the dye) and consequently this state is kept away from the dcbpy ligand that anchors at the TiO_2 surface, thus favoring a slow charge recombination with the semiconductor's conduction band electrons. Yet, the two new dyes (Ru–Cl and Ru–NCS) do not present significant differences regarding the discussed point. Someone could expect that the dye, containing the isothiocyanato ligand, would present similar with N3 behavior. This would be the case if the NCS ligand made a contribution to the HOMOs of the Ru–NCS dye. This aspect will be further discussed in the following section.

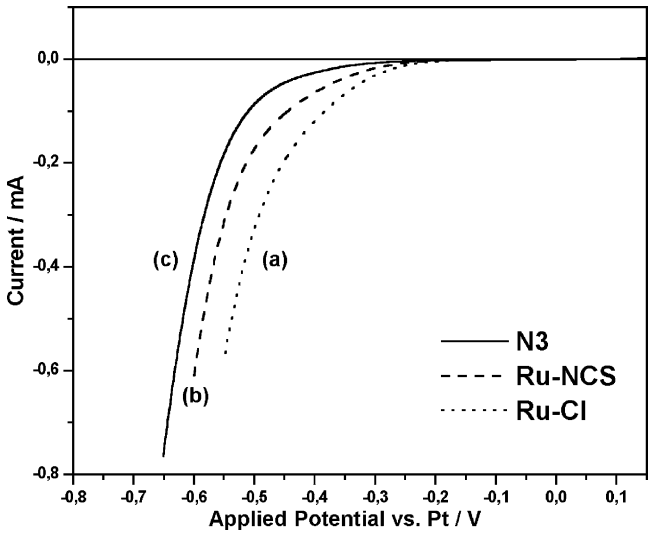

Fig. 5. Cyclic voltammograms (CV) in the dark, for Ru–Cl (a), Ru–NCS (b), and N3 (c) dyes, respectively, of the DSSCs using the redox polymer electrolyte. Photoelectrode area: 0.3 cm^2, scan rate: 20 mV s^{-1}.

3.7. Construction of the energetic diagram of the DSSCs

The kinetics of all the reactions taking place in a DSSC are dependent upon the energies of the dye excited/ground state oxidation potentials in relation with the lower bound of the semiconductor's conduction band. Hence, the overall energetic diagram was constructed (Fig. 6) by making the following approximations: first, the sensitizer's energetics are not too different whether it is in solution or adsorbed to TiO_2 and second, the redox couple's energetics are similar whether the electrolyte is solid or liquid.

Cyclic voltammograms of the Ru–Cl and Ru–NCS complexes showed well-defined reversible oxidation-reduction waves, revealing the values of the oxidation potentials for

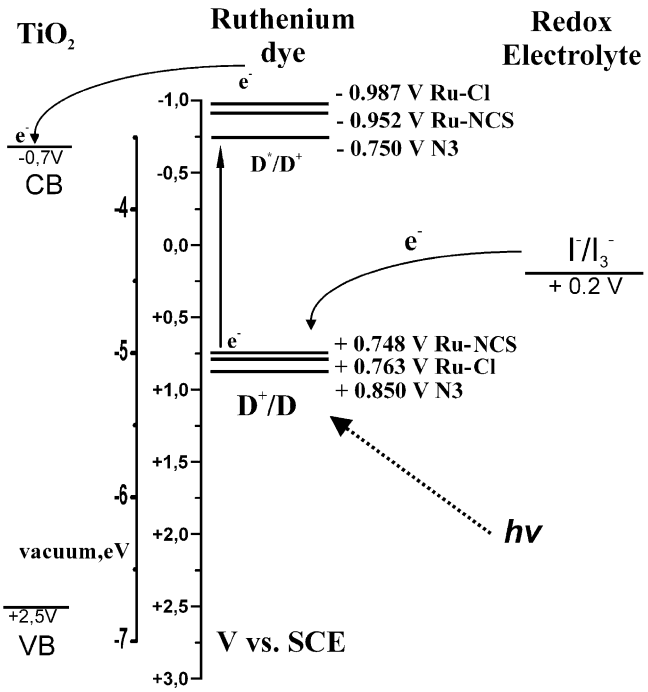

Fig. 6. Energy level diagram for DSSCs using different Ru-dyes.

the Ru^{3+}/Ru^{2+} couple to be +0.810 and +0.795 V versus Ag/AgCl, respectively. The oxidation potentials E^0 (Ru^{2+}/Ru^{3+}) express the process of reduction of the oxidized dye by the I^- ions, and thus, give straightforward values for the HOMO energy levels of the two complexes [39]. These were +0.763 V for Ru–Cl dye and +0.748 versus SCE for the second Ru–NCS dye.

One may observe that the two oxidation potentials are less positive than the corresponding potential of the standard N3 dye (+0.85 V versus SCE, as seen from Table 1) due to the presence of bdmpp ligand which is a stronger σ-donor than dcbpy, stabilizing the oxidized form of the Ru metal ion. That is, the Ru(II) → Ru(III) process (metal oxidation reaction) becomes more favorable for the two new complexes than in the case of N3 dye. Still, the oxidation potentials for the two new dyes are almost equal, although someone would expect that the Ru–NCS complex would have a more positive redox potential due to the isothiocyanato ligand π-acceptor properties and corresponding π-donor properties of chloride ligand. These ligands do not seem to have an important contribution on the HOMOs of the complex. The above result leads us to the conclusion that the positive charge is mainly localized on the metal, thus favoring a rapid charge recombination with the semiconductor's conduction band electrons (Eq. (11)).

Table 1
HOMO–LUMO energies of Ru–Cl and Ru–NCS complexes and band gap values obtained from calculations derived from cyclic voltammetry measurements of the complexes in CH_3CN and absorption properties of the dyes adsorbed on TiO_2 substrate

Dye	HOMO (*V* vs. SCE)	LUMO (*V* vs. SCE)	Band gap (eV)
Ru–Cl	+0.763	−0.987	1.75
Ru–NCS	+0.748	−0.952	1.70
N3	+0.850	−0.750	1.60

Literature data for the N3 dye [27] are presented for comparison.

The oxidation of the excited dye through electron injection into the conduction band of TiO_2 is described by the E^0 (Ru^{2+*}/Ru^{3+}) redox potential, given by Eq. (12):

$$E^0\left(\frac{Ru^{2+*}}{Ru^{3+}}\right) = E^0\left(\frac{Ru^{2+}}{Ru^{3+}}\right) - \Delta E_{0-0} \quad (12)$$

where ΔE_{0-0} corresponds to the transition energy between the lowest vibrational levels in the ground and excited state [28]. The 0−0 excitation energy of the dyes adsorbed on TiO_2 is determined from the absorption threshold of their lowest-energy MLCT bands (derived from the low energy tail of the absorption spectrum, right Fig. 2). These thresholds are about 710, 750, and 775 nm for Ru–Cl, Ru–NCS, and N3 dyes, respectively, corresponding to potentials of +1.75 and +1.70, and 1.60 eV, correspondingly. Thus, the first reduction potentials of the Ru^{3+}/Ru^{2+} couple can be obtained from Eq. (12), i.e. the first excited energy levels of the dyes lie at −0.987, −0.902, and −0.750 V for the Ru–Cl, Ru–NCS, and N3 complexes, respectively (all the data obtained are summarized in Table 1).

In Fig. 6, the conduction band potential of TiO_2 lies at −0.7 V vs. SCE [27,31]. It is clear that electron injection from the excited dyes molecules into the conduction band of the semiconductor is thermodynamically possible, as the driving force for charge displacement into the oxide is about 0.25–0.3 eV for the new dyes, whilst for N3 is only 0.05 eV. The excited state of N3 dye matches better the lower bound of the conduction band of the semiconductor than the LUMOs of the Ru–Cl and Ru–NCS complexes, thus minimizing the energetic losses during the electron transfer process. The better overlap is believed to play a crucial role making more favorable the electron injection [40]. This is supported by the experimental results showing that the IPCE values for N3 dye are higher than that obtained with the Ru–Cl and Ru–NCS dyes, in agreement with the calculated electron injection efficiencies (ϕ_{inj}), Section 3.3.

Fig. 6 shows that the dye regeneration is also a thermodynamically favourable process, as the redox potential of I^-/I_3^- redox couple lies at +0.2 V versus SCE [30] (above the HOMO energy levels of all three complexes). The reduction of dye cations is easier for the N3 complex, since the larger driving force (distance between the D^+/D and I^-/I_3^- potential levels) leads to a better electron transfer from the iodide ions. In the case of N3 dye, Nazeeruddin et al. postulated that the isothiocyanato ligand might stabilize the hole generated on the Ru-metal after having injected an electron into the conduction band [41]. This assumption was further supported by the fact that the outermost orbitals of the complex might contain a significant amount

of S3p-character from this ligand pointing in the direction of the electrolyte, and thus facilitating the dye regeneration [42].

4. Conclusions

An attempt was made to design and synthesize efficient molecular sensitizers for regenerative nanocrystalline solar cells. Our strategy to combine chromophoric ligands with well optimized π^* energies together with appropriate ancillary ligands led us to the synthesis of complexes exhibiting interesting light harvesting properties with high extinction coefficients. The performance of the new complexes was significantly lower than that of the classical N3 dye due to poorer IPCE values as well as to reduced I_{sc} and V_{oc} values. This can be explained in terms of reduced injection efficiencies, less favorable energetics of ground/excited states, an enhancement in the rate of the recombination of dye holes with conduction band electrons (probably due to non significant involvement of the non-chromophoric ligands on the frontier orbitals of the complexes), and an increase of the dark current passing through the cell.

The replacement of only one non-chromophoric ligand (–Cl) by the isothiocyanato ligand led to a three times increase of the overall energy conversion efficiency of the corresponding DSSCs. The –NCS ligand slightly altered the spectral absorption of the complex and the energetics of ground/excited states. The above increase resulted from a large enhancement of IPCE and short-circuit photocurrent (I_{sc}) values, mainly attributed to better electron injection efficiencies. Moreover, the second dye exhibited superior V_{oc} values (about 90 mV higher), due to lower dark current magnitude.

These results must be taken into account in the conception and design of new strategy concerning the synthesis of ruthenium complexes for DSSCs. The combination of only one polypyridyl ligand (bidentate or tridentate) with low lying π^*-orbitals possessing carboxyl groups (for the anchoring on TiO_2 surface) together with a suitable number of isothiocyanate ligands, could lead to high energy conversion efficiencies. Work in this direction is currently under progress using novel azo-aromatic ligands recently developed in our laboratory.

Acknowledgements

This work has been supported by Greek-German bilateral cooperation project. Thanks must be addressed to Prof. V.J. Catalano for providing the bdmpp ligand and to Dr. Katerina Chryssou for the synthesis of the bdmpp complexes and to Dr. H. Cachet for helpful discussions. Delis AE Athens-Greece and Degussa AG Frankfurt-Germany are also greatly acknowledged for generously supplying the TiO_2 P25 powder.

References

[1] B. O'Regan, M. Grätzel, Nature (Lond.) 353 (1991) 737.
[2] M.K. Nazeeruddin, A. Kay, I. Rodicio, R. Humphry-Baker, E. Müller, P. Liska, N. Vlachopoulos, M. Grätzel, J. Am. Chem. Soc. 115 (1993) 6382.
[3] M. Grätzel, Sensitized Nanocrystalline Solar Cells, Personal Communication, Athens, Greece, 24 May 2001.
[4] M.K. Nazeeruddin, P. Pechy, T. Renouard, S.M. Zakeeruddin, R. Humphry-Baker, P. Comte, P. Liska, L. Cevey, E. Costa, V. Shklover, L. Spiccia, G.B. Deacon, C.A. Bignozzi, M. Grätzel, J. Am. Chem. Soc. 123 (2001) 1613.
[5] V.J. Catalano, R. Kurtaran, R.A. Heck, A. Ïhman, M.G. Hill, Inorg. Chim. Acta 286 (1999) 181.
[6] C.A. Bignozzi, R. Argazzi, C.J. Kleverlaan, Chem. Soc. Rev. 29 (2000) 87.
[7] G. Katsaros, T. Stergiopoulos, I.M. Arabatzis, K.G. Papadokostaki, P. Falaras, J. Photochem. Photobiol. A 149 (2002) 191.
[8] T. Stergiopoulos, I.M. Arabatzis, G. Katsaros, P. Falaras, Nano Lett. 2 (11) (2002) 1259.
[9] O. Kohle, S. Ruile, M. Grätzel, Inorg. Chem. 35 (16) (1996) 4779.
[10] I.M. Arabatzis, T. Stergiopoulos, G. Katsaros, M.C. Bernard, D. Labou, S.G. Neofytides, P. Falaras, Appl. Catal. B: Environ. 42 (2003) 187.
[11] K. Chryssou, V.J. Catalano, R. Kurtaran, P. Falaras, Inorg. Chim. Acta 328 (2002) 204.
[12] K. Chryssou, T. Stergiopoulos, P. Falaras, Polyhedron 21 (2002) 2773.
[13] G. Franco, L.M. Peter, E.A. Ponomarev, Electrochem. Commun. 1 (1999) 61.
[14] T. Trupke, P. Wurfel, I. Uhlendorf, J. Phys. Chem. B 104 (2000) 11484.
[15] T. Stergiopoulos, I.M. Arabatzis, H. Cachet, P. Falaras, J. Photochem. Photobiol. A 155 (2003) 163.
[16] P.A. Anderson, G.F. Strouse, J.A. Treadway, F. Richard Keene, T.J. Meyer, Inorg. Chem. 33 (1994) 3863.
[17] P. Falaras, Sol. Energy Mater. Sol. Cells 53 (1998) 163.
[18] G. Smestad, Optoelectronics of Solar Cells, SPIE Press, Bellingham, Washington, 2002.
[19] A. Islam, H. Sugihara, H. Arakawa, J. Photochem. Photobiol. A 158 (2003) 131.
[20] A.C. Fisher, L.M. Peter, E.A. Ponomarev, A.B. Walker, K.G.U. Wijayantha, J. Phys. Chem. B 104 (2000) 949.
[21] T. Stergiopoulos, H. Cachet, P. Falaras, in: The 203th Meeting of The Electrochemical Society Inc., Paris, France, April 27 to May 2 2003, Abstract No. 1729.
[22] A. Fillinger, B.A. Parkinson, J. Electrochem. Soc. 146 (12) (1999) 4559.
[23] J.B. Ashbury, N.A. Anderson, E. Hao, X. Ai, T. Lian, J. Phys. Chem. B 107 (2003) 7376.
[24] M.T. Indelli, C.A. Bignozzi, F. Scandola, J.P. Collin, Inorg. Chem. 37 (1998) 6084.
[25] P. Qu, D.W. Thompson, G.J. Meyer, Langmuir 16 (2000) 4662.
[26] A.C. Khazraji, S. Hotchadani, S. Das, P.V. Kamat, J. Phys. Chem. B 103 (1999) 4693.
[27] A. Hagfeldt, M. Grätzel, Chem. Rev. 95 (1995) 49.
[28] R. Memming, Semiconductor Electrochemistry, Wiley-VCH Verlag Gmbh, D-69469 Weinheim, 2001.
[29] A. Vittadini, A. Seloni, F.P. Rotzinger, M. Grätzel, Phys. Rev. Lett. 81 (1998) 2954.
[30] A.J. Bard, R. Parsons, J. Jordan, Standard Potentials in Aqueous Solution, Marcel Dekker, New York, 1985.
[31] G. Redmond, D. Fitzmaurice, J. Phys. Chem. 97 (1993) 1426.
[32] P. Salvador, J. Phys. Chem. B 105 (2001) 6128.
[33] S.Y. Huang, G. Schlichthörl, A.J. Nozik, M. Grätzel, A.J. Frank, J. Phys. Chem. B 101 (1997) 2576.
[34] A. Stanley, D. Matthews, Aust. J. Chem. 48 (1995) 1293.

[35] F. Pichot, B.A. Gregg, J. Phys. Chem. B 104 (2000) 6.
[36] H. Greijer Angrell, J. Lindgren, A. Hagfeldt, Sol. Energy 75 (2003) 169.
[37] Y. Tachibana, K. Hara, S. Takano, K. Sayama, H. Arakawa, Chem. Phys. Lett. 36 (2002) 297.
[38] Y. Tachibana, S.A. Haque, I.P. Mercer, J.E. Moser, D.R. Klug, J.R. Durrant, J. Phys. Chem. B 105 (2001) 7524.
[39] H. Rensmo, S. Lunell, H. Siegbahn, J. Photochem. Photobiol. A 114 (1998) 117.
[40] K. Srikanth, V.R. Marathe, M.K. Mishra, Int. J. Quantum Chem. 89 (2002) 535.
[41] Md.K. Nazeeruddin, M. Grätzel, J. Photochem. Photobiol. A 14 (2001) 579.
[42] A. Hagfeldt, M. Grätzel, Acc. Chem. Res. 33 (2000) 269.